Am J Transl Res 2024;16(10):5441-5453
www.ajtr.org /ISSN:1943-8141/AJTR0156361

Original Article

Morinda officinalis saponins promote osteogenic differentiation of human umbilical cord-derived mesenchymal stem cells via the BMP-SMAD signaling pathway

Jian Zhou[1,2*], Fanru Zhou[1*], Liu Yang[1*], Haihui Liang[1*], Qinyao Zhu[1], Fenghua Guo[3], Xiushan Yin[1], Jian Li[2,4]

[1]*Applied Biology Laboratory, College of Pharmaceutical and Biological Engineering, Shenyang University of Chemical Technology, Shenyang 110142, Liaoning, China;* [2]*College of Pharmaceutical Sciences, Gannan Medical University, Ganzhou 341000, Jiangxi, China;* [3]*Glabiolus Biotech (Xuzhou) Co., Ltd., Xuzhou 221000, Jiangsu, China;* [4]*Glabiolus Biotech (Jiangxi) Co., Ltd., Ganzhou 341005, Jiangxi, China.* [*]*Equal contributors and co-first authors.*

Received March 5, 2024; Accepted August 19, 2024; Epub October 15, 2024; Published October 30, 2024

Abstract: Background: *Morinda officinalis* saponins (MOS), a traditional Chinese medicine extracted from *M. officinalis* roots, have been used as a health supplement. Existing evidence suggests that extracts from this plant can be used for osteoporosis treatment. However, the molecular mechanisms underlying the anti-osteoporotic effects of *M. officinalis* remain poorly understood. Methods and Results: In this study, we investigated the osteogenesis-promoting effects of MOS on human umbilical cord-derived mesenchymal stem cells (HUC-MSCs). Alkaline phosphatase staining, alizarin red staining, and quantitative reverse transcription-PCR demonstrated that MOS promoted the osteogenic differentiation of HUC-MSCs in a concentration-dependent manner. RNA sequencing results showed that the expression of key osteogenic differentiation-related genes, including *BMP4*, as well as the activity of transforming growth factor-β and calcium signaling pathways increased following MOS treatment. Furthermore, treatment with the bone morphogenetic protein (BMP) antagonist Noggin reversed the MOS-induced pro-osteogenic differentiation effects and the upregulation of osteoblast-specific markers. Conclusions: Overall, the results indicate that MOS can partially promote osteogenic differentiation of HUC-MSCs by regulating the BMP-SMAD signaling pathway. These findings indicate the potential utility of MOS as a therapeutic agent for osteoporosis, particularly in the context of stem cell therapy.

Keywords: *Morinda officinalis* saponins, human umbilical cord-derived mesenchymal stem cells, osteogenic differentiation, RNA sequencing, stem cell therapy

Introduction

Mesenchymal stem cells (MSCs), which are capable of osteogenic, chondrogenic, and adipogenic lineage commitment, are multipotent cells obtained from adipose tissue, bone marrow, umbilical cord, and Wharton's jelly (WJ) [1-3]. Owing to their functions, such as tissue repair, hematopoietic support, and immunomodulation, MSCs are considered ideal seed cells for different treatments [4]. They exhibit promising potential for the clinical treatment of multi-organ injuries owing to their low immunogenicity, extensive and convenient availability, sufficient quantity, robust differentiation ability, rapid proliferation, comprehensive application prospects, and absence of ethical controversy [3, 5-7]. Human umbilical cord-derived mesenchymal stem cells (HUC-MSCs), which are isolated from the human umbilical cord, have the ability to differentiate into various cell types, rendering them a promising candidate for cell-based therapy [8]. HUC-MSCs are currently used in the treatment of various diseases, such as osteoarthritis, diabetes and related complications, systemic lupus erythematosus, and viral infections [9]. Moreover, HUC-MSCs can be used as a noninvasive treatment for COVID-19 [10]. These clinical applications suggest their promising role in regenerative medicine in the future.

https://doi.org/10.62347/KNRS3234

Morinda officinalis, a dicotyledonous plant widely grown in tropical and subtropical regions of the world, is one of the most well-known Chinese herbs. Recognized for over 2000 years in Northeast Asia, its roots have the ability to bolster the immune system and fortify the bones and kidneys, as documented in the Chinese pharmacopeia [11]. The herb has been commonly used to treat rheumatoid arthritis, impotent dermatitis, and menstrual disorders [12, 13]. Recent research has unveiled various pharmacological effects of *M. officinalis*, including immunomodulation, anti-tumor, anti-aging, and anti-fatigue properties [14, 15]. *M. officinalis* root extracts can promote bone formation *in vivo* and exhibit beneficial effects in the prevention and treatment of osteoporosis [13, 16]. *Morinda officinalis* saponins (MOS) are important active ingredients of *M. officinalis* and are currently mainly used as nutraceuticals. Despite numerous experimental studies demonstrating the beneficial effects of *M. officinalis* extracts, particularly polysaccharides and oligosaccharides, on the promotion of osteoblast proliferation and activity, induction of osteogenic differentiation in bone marrow MSCs, and bone metabolism [17-19], the effects of MOS on HUC-MSCs remain unexplored. In this study, we investigated the effects of MOS on the proliferation and osteogenic differentiation of HUC-MSCs and the resulting transcriptomic changes.

Materials and methods

Media and reagents

MOS was purchased from Xi'an Yatu Biotechnology Co., Ltd. (Xi'an, China), stored in sealed ziplock bags in a dry environment, and preserved at -20°C after dissolving in water. HUC-MSCs were supplied by Biotech & Biomedicine Group., Ltd. (Shenyang, China). Dulbecco's modified Eagle's medium (DMEM), α-minimum essential medium (MEM), and penicillin (10000 Units/mL)/streptomycin (10000 μg/mL) (P/S) were purchased from Gibco (Grand Island, NY, USA). Fetal bovine serum (FBS) was sourced from ExCell Company (Shanghai, China), while L-glutamine (200 mM) was purchased from Sangon Biotech (Shanghai, China). The BCIP/NBT alkaline phosphatase (ALP) color development kit was purchased from Beyotime Biotechnology (Shanghai, China), and the cell counting kit-8 (CCK-8) was purchased from Dojindo Laboratories (Kumamoto, Japan). Alizarin red staining kit was procured from Beijing Solarbio Science & Technology Co., Ltd. Additionally, β-glycerophosphate disodium salt hydrate and ascorbic acid were acquired from Sigma-Aldrich (St. Louis, MO, USA). Recombinant human bone morphogenetic protein 4 (BMP4) was purchased from PeproTech (Rocky Hill, NJ, USA), and Noggin was obtained from MedChem Express (Monmouth Junction, NJ, USA).

Cell culture

HUC-MSCs were cultured and maintained in DMEM complete medium (DMEM supplemented with 10% FBS, 1% P/S, and 1% L-glutamine) in a 5% CO_2 humidified incubator at 37°C until 80% confluence was reached. HUC-MSCs from passages 4 to 6 were used for all experiments, and the complete medium was replaced every two days.

Morphological characteristics and cytotoxicity test

HUC-MSCs (5×10^5 cells/well, passages 6) were seeded onto 12-well plates and incubated for 24 h. Subsequently, the experimental groups were treated with six different concentrations of MOS (0, 4, 20, 100, 500, and 2500 μg/mL) for 1, 6, 24, and 48 h. Cell morphology was observed and morphological data were collected using an inverted microscope (S80-SLIDER, Leica Microsystems, Wetzlar, Germany). Cytotoxic effects of MOS on HUC-MSCs were determined using the CCK-8 kit. Briefly, HUC-MSCs (5×10^3 cells/well, passage 6) were seeded in 96-well plates and incubated for 24 h, followed by culturing with different MOS concentrations (0, 5, 25, 50, 100, and 200 μg/mL) for 24, 48, 72, and 96 h, with three parallel control wells in each group. Subsequently, 10 μL CCK-8 reagent was added to each well, the plates were incubated for 3 h in a 5% CO_2 humidified incubator at 37°C, and the absorbance was measured at 450 nm.

Osteoblast differentiation assay

For *in vitro* HUC-MSC differentiation, passage 5 HUC-MSCs were plated at a density of 1.0×10^5 cells/well in 12-well plates. Cells were cultured in complete medium until they reached a

Table 1. Primer sequences used for quantitative reverse transcription-PCR-based analysis of gene expression

Gene name	Accession No.	Primer Sequence (5' to 3')
Runx2	NM_001024630.4	F: GACAAGCACAAGTAAATCATTGAACTACAG
		R: GTAAGGCTGGTTGGTTAAGAATCTCTG
Ocn	NM_198406.3	F: ACCAGGTAATGCCAGTTTGC
		R: CCCCCTCTAGCCTAGGACC
Opn	NM_001040058.2	F: CTGAAACCCACAGCCACA
		R: TGTGGAATTCACGGCTGA
Gapdh	NM_002046.7	F: AGCCACATCGCTCAGACAC
		R: GCCCAATACGACCAAATCC

confluence of 80%; subsequent replacement with phosphate-buffered saline (PBS) preceded the introduction of osteogenic differentiation medium. Osteogenic media (OM), comprising α-MEM, 5% FBS, 1% P/S, 100 μg/mL ascorbic acid, 5 mM β-glycerophosphate disodium salt hydrate, and varying concentrations of MOS (5, 25, 50, and 100 μg/mL), were used for differentiation. The media were replaced every two days, and three biological replicates were set for each group.

ALP and alizarin red staining assays

At the initial stage of osteogenic differentiation of HUC-MSCs (seven days), cells were stained using an ALP staining kit. After medium removal, the cells were washed with PBS, fixed in 4% paraformaldehyde for 15 min, and washed thrice with PBS. Subsequently, the cells were stained with an ALP staining solution and incubated in the dark at 30°C for 12 h. To investigate the effect of MOS on mineralization, alizarin red staining was performed at the late stage of osteogenic differentiation (21 days). After staining with a 0.2% alizarin red solution for 30 min at room temperature, the reaction was terminated by washing the HUC-MSCs gently with ultrapure water; the cells were then observed under a microscope (DS-Ri2, Nikon, Tokyo, Japan). The positive cell area was quantified using ImageJ v1.52 (National Institutes of Health, Bethesda, MD, USA).

Quantitative reverse transcription-PCR (RT-qPCR)

Total RNA was extracted from HUC-MSCs using TRIzol reagent (Vazyme, Nanjing, China) according to the manufacturer's instructions. Briefly, passage 5 HUC-MSCs were plated at a density of 1.0×10^5 cells per well in six-well plates, and each well received 500 μL TRIzol reagent after five days of osteogenic differentiation induction. After centrifugation for 10 min at 12000 × *g* and 4°C, the supernatants were collected for subsequent RNA isolation. cDNA was synthesized using the Prime-Script RT Reagent Kit (TaKaRa Biotech, Tokyo, Japan). The mRNA levels of osteogenic differentiation markers (*RUNX2*, *OCN*, and *OPN*) were determined via RT-qPCR using SYBR Premix Ex Taq (TaKaRa Biotech) and Bio-Rad CFX 96 real-time PCR detection system (Hercules, CA, USA) with QuantStudio™ Design and Analysis Software v1.4.3 (Thermo Fisher Scientific, Waltham, MA, USA). All primer sequences for the tested genes are listed in **Table 1**. The cycling conditions were as follows: denaturation at 95°C for 1 min, followed by 40 cycles at 95°C for 15 s, 60°C for 15 s, and 72°C for 45 s. The successful generation of individual amplicons was confirmed through melting curve analysis. Gene expression levels were determined using the $2^{-\Delta\Delta Cq}$ method and normalized to *GAPDH* levels [20].

RNA sequencing (RNA-seq) analysis

The cells were sub-cultured in a 6-cm dish once the viability of HUC-MSCs revived in a 10 cm dish reached 90%. HUC-MSCs were cultured with 25 μg/mL MOS for 48 h; a normal control group (complete medium without MOS) was also established, with three parallel wells in each group. The cell pellets were washed, collected, and sent to Shenzhen Promegene Technology Co., Ltd. (Shenzhen, China) for sequencing. All purified libraries were sequenced on DNBSEQ-T7RS using Geneplus to acquire 150 bp paired-end sequence reads. Raw RNA-seq data were deposited in the NCBI Sequence Read Archive database (https://www.ncbi.nlm.nih.gov/sra/PRJNA843361).

Western blotting

HUC-MSCs were inoculated into six-well plates and subsequently cultured with OM+BMP4, OM+BMP4+Noggin, OM+Noggin, OM+MOS, OM+MOS+Noggin, or OM medium for 24 h. The

cells were lysed with the standard radioimmunoprecipitation assay lysis buffer supplemented with 1 mM phenylmethylsulfonyl fluoride (PMSF), and the extracted proteins were separated using 10% sodium dodecyl sulfate polyacrylamide gel electrophoresis. Following electrophoresis, the resolved proteins were transferred onto polyvinylidene difluoride membranes, which were blocked with 5% non-fat milk and incubated with primary antibodies against p-SMAD1/5/9 (Cell Signaling Cat# 13820) and beta-actin (Sigma-Aldrich Cat# A1978). Thereafter, the membranes were washed and probed with an anti-rabbit secondary antibody (R&D Systems). Finally, the membranes were examined using an enhanced chemiluminescence detection system (Beyotime Cat# P0018AS) and visualized with a Bio-Rad imaging system (Hercules, CA, USA).

Statistical analysis

Cell experiments were repeated three times. All values are presented as mean ± standard deviation. Significant differences were determined using a one-way analysis of variance followed by Dunnett's or Tukey's multiple comparison test. GraphPad Prism 9.0 (GraphPad Software Inc., La Jolla, CA, USA) was used to perform data analysis and statistical tests, while edgeR package v3.26.8 (Bioconductor, Roswell Park Cancer Institute, Buffalo, NY, USA) was used to identify differentially expressed genes (DEGs). DEGs were evaluated based on the following criteria: (i) more than 1.41-fold change in gene expression and (ii) $P < 0.05$. The fold change in the expression of each gene was calculated by comparing the standardized read counts of MOS-treated cells with those of the non-treated cells (fold change = standardized read counts of MOS-treated cells/standardized read counts of non-treated cells). Log_2(fold change) was used for convenience, where $|Log_2(\text{fold change})| > 1$ indicated at least a twofold change. **P*-values < 0.05 were considered statistically significant.

Results

MOS administration dose for HUC-MSCs

The cytotoxicity of various MOS concentrations to HUC-MSCs was tested to determine the appropriate concentration for this study. An analysis of the cells under a microscope revealed that cell death was evident after 1 h when MOS concentration exceeded 500 μg/mL, indicating significant toxicity to HUC-MSCs at this concentration (**Figure 1A**). CCK-8 assay results showed that the proliferation of HUC-MSCs was not affected by low MOS concentrations (5 and 25 μg/mL). However, MOS concentrations of 50 and 100 μg/mL were toxic to HUC-MSCs, leading to the inhibition of cell proliferation (**Figure 1B**). Therefore, the 200 μg/mL concentration of MOS was defined as the sublethal concentration.

MOS promoted the osteogenic differentiation and mineralization of HUC-MSCs

The ALP staining assay (**Figure 2A**, **2B**) showed that MOS treatment resulted in an increase in the number of ALP-positive cells in a dose-dependent manner after seven days of osteogenic differentiation. Alizarin red staining was used to investigate the effects of MOS on calcium nodule formation after 21 days (**Figure 2C**, **2D**). Notably, the number of calcium nodules significantly increased following treatment with MOS and was positively correlated with MOS concentration. A comparative analysis of ALP and alizarin red staining revealed a significant positive effect of MOS on the osteogenic differentiation of HUC-MSCs. The effect of MOS on HUC-MSCs was more pronounced at a concentration of 100 μg/mL. The expression of the osteogenic differentiation markers *RUNX2*, *OCN*, and *OPN* in the MOS-treated group was significantly increased ($P < 0.05$) compared with that in the control group (**Figure 2E**).

Potential mechanisms underlying the effects of MOS on the osteogenic differentiation of HUC-MSCs based on RNA-seq analysis

To further investigate the potential mechanisms underlying MOS-induced osteogenic differentiation in HUC-MSCs, we analyzed the gene expression profiles of HUC-MSCs cultured with and without MOS (25 μg/mL) using RNA-seq. To determine significant differences between the MOS-treated (M25) and non-treated (M0) samples, we performed 3D principal component analysis (PCA) to reduce dimensionality and evaluate the independence of each group (**Figure 3A**). The PCA results showed that M25 and M0 were divided into two distinct groups. The cumulative contribution rates for

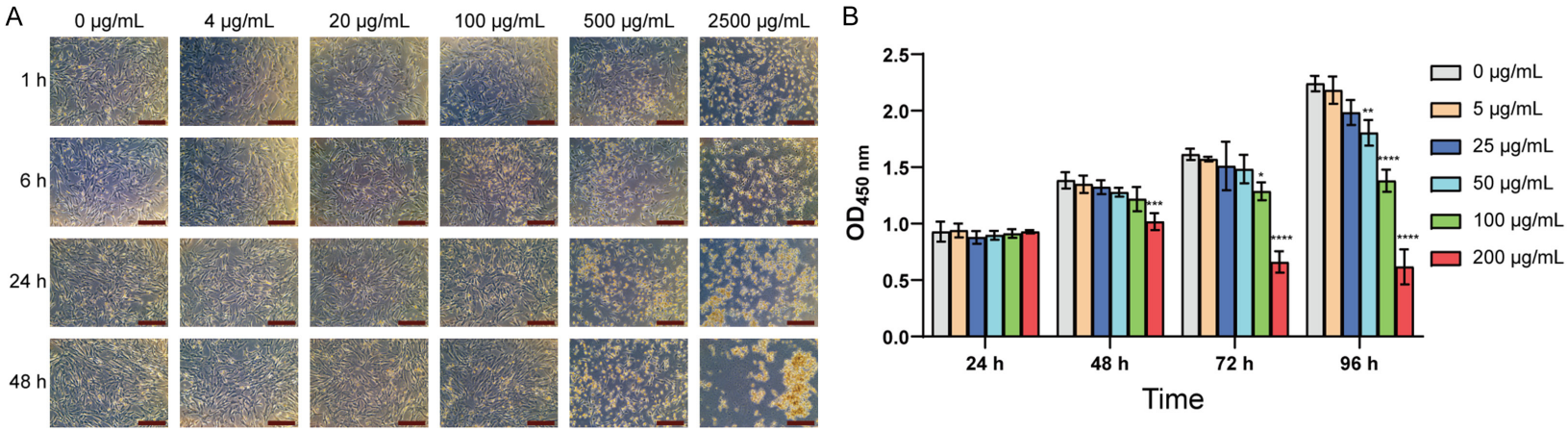

Figure 1. MOS affects HUC-MSC proliferation. A. The cells grew within 48 h of treatment with a particular MOS concentration (magnification: × 40, scale bar: 500 μm). B. CCK-8 assay results showing cell viability within 96 h of treatment with different MOS concentrations. *P < 0.05*; all values are presented as mean ± SD; n = 3 (vs. 0 μg/mL group; **P* < 0.05, ***P* < 0.01, ****P* < 0.001, *****P* < 0.0001). Significant differences compared with those in the 0 μg/mL group were analyzed using a one-way ANOVA with Dunnett's post-hoc test. MOS: *Morinda officinalis* saponins; HUC-MSCs: human umbilical cord-derived mesenchymal stem cells; CCK-8: cell counting kit-8; SD: standard deviation.

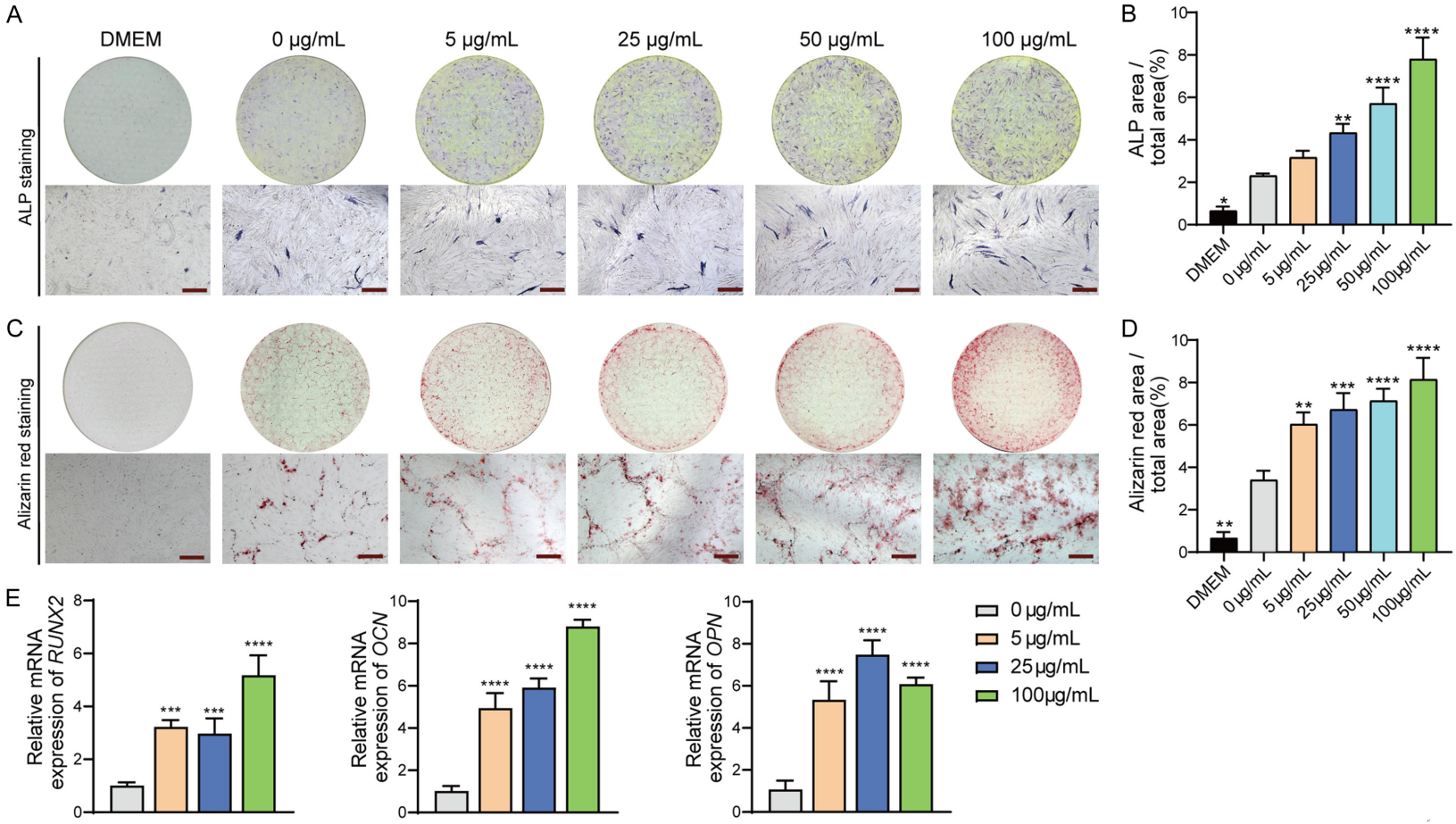

Figure 2. MOS promotes HUC-MSC osteogenic differentiation and mineralization in a concentration-dependent manner. A and B. HUC-MSCs were cultured in DMEM complete medium and osteogenic differentiation medium with and without MOS for seven days, respectively. ALP staining assay was performed, and the staining area was quantified using ImageJ. C, D. HUC-MSCs were cultured for 21 days. Alizarin red staining results; the stained area was quantified using ImageJ; the orange-red dots represent calcium nodules. E. Expression of osteogenic markers. Data are presented as mean ± SD; n = 3 (vs. 0 μg/mL group; **P* < 0.05, ***P* < 0.01, ****P* < 0.001, *****P* < 0.0001). Significant differences compared with those in the 0 μg/mL group were analyzed using one-way ANOVA with Dunnett's post-hoc test. Magnification: × 40, scale bar: 500 μm. MOS: *Morinda officinalis* saponins; HUC-MSCs: human umbilical cord-derived mesenchymal stem cells; DMEM: Dulbecco's modified eagle medium; ALP: alkaline phosphatase; SD: standard deviation.

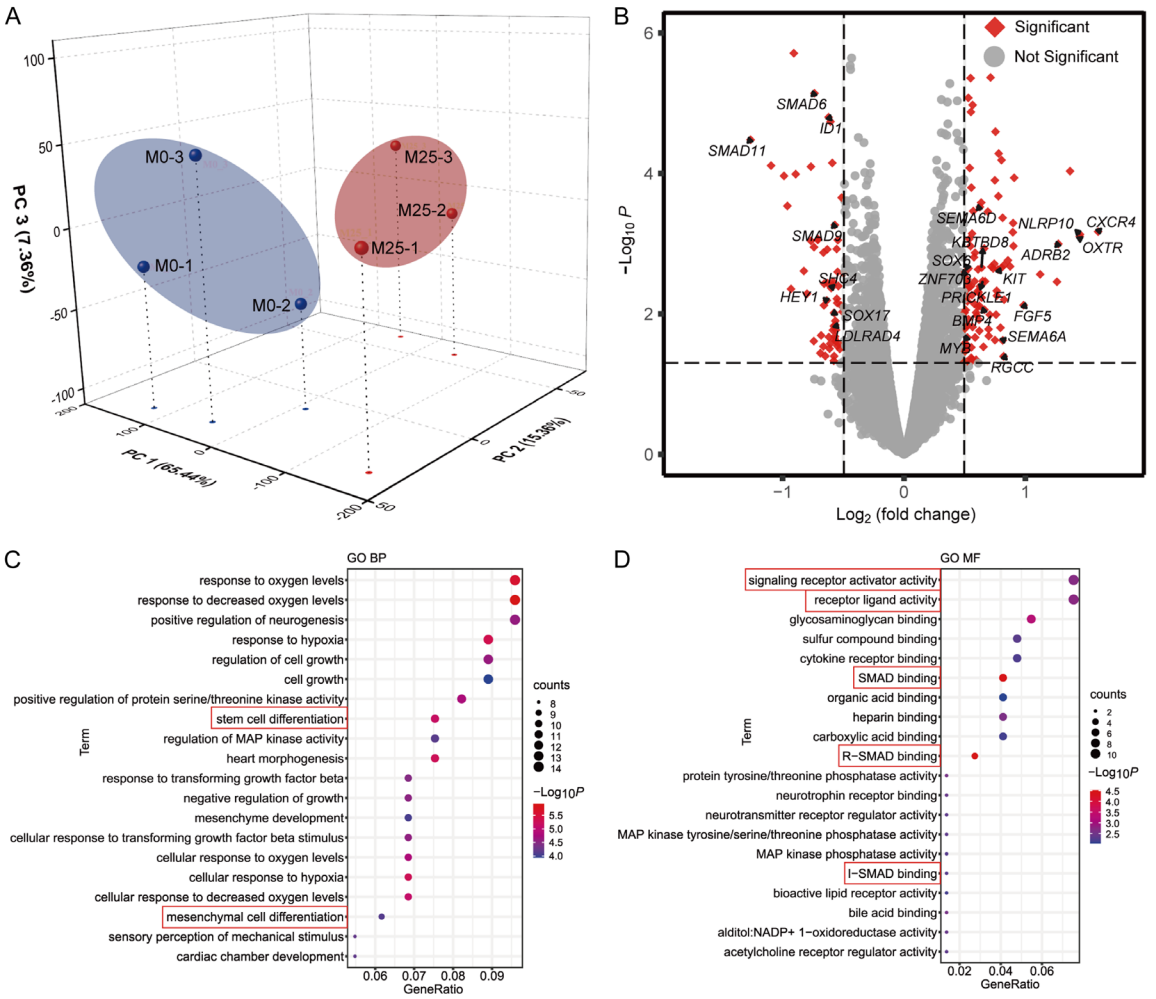

Figure 3. RNA sequencing analysis results. A. The 3D principal component analysis of six experimental samples was visualized based on MOS-treated (M25, red) and non-treated (M0, blue) samples. B. A volcano plot showing differential gene expression and annotations of significantly upregulated or downregulated differentially expressed genes (red). C, D. GO enrichment analysis of terms in the biological process (BP) and molecular function (MF) categories; the ontologies represent the top 20 significantly enriched terms in each category. MOS: *Morinda officinalis* saponins; GO: Gene Ontology.

each principal component on the vertical axis were 65.44%, 15.38%, and 7.36% for PC1, PC2, and PC3, respectively, indicating that the three principal components were sufficient for distinguishing the two groups.

Next, we compared differences in gene expression between the control and MOS-treated groups using edgeR. A total of 165 DEGs were identified based on a threshold of (false discovery rate $|\log_2(\text{fold change})| > 0.5$ and $P < 0.05$), with 104 and 61 DEGs being upregulated and downregulated, respectively, in the MOS-treated group. Volcano plots showing the number of DEGs identified after screening and the genes associated with osteogenic differentiation are shown in **Figure 3B**. The expression levels of osteogenic differentiation genes based on the RNA-seq data are summarized in Tables S1 and S2.

To further investigate the functional states of HUC-MSCs and potential molecular regulators after MOS treatment, the DEGs were subjected to Gene Ontology (GO) and Kyoto Encyclopedia of Genes and Genomes (KEGG) analyses. DEGs were significantly enriched in biological process (BP) terms (**Figure 3C**), stem cell and mesenchymal cell differentiation. In the context of stem cell differentiation, specific terms exhibited significant enrichment, with upregulated genes (*BMP4, EDN1, KBTBD8, KIT,*

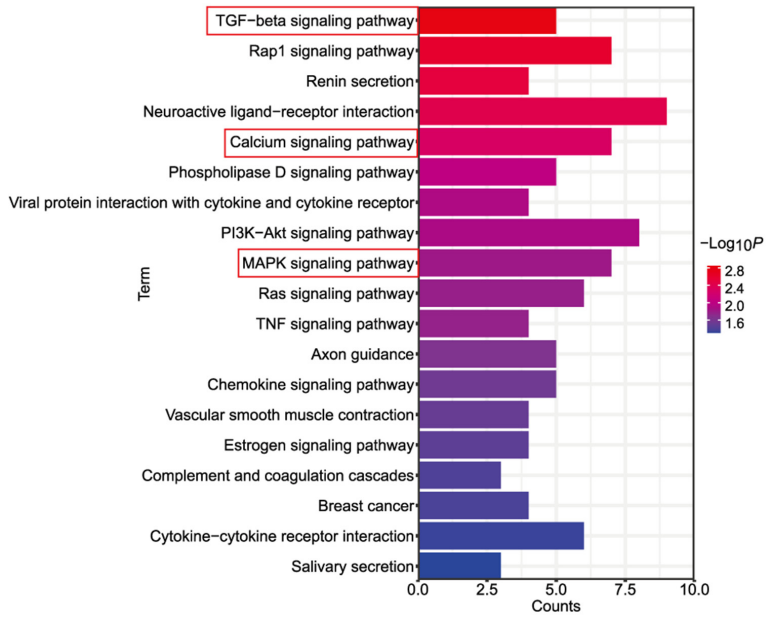

Figure 4. KEGG pathway enrichment analysis results. The top 19 significantly enriched pathways were ranked by gene count. Three of the pathways, namely, the TGF-β, calcium, and MAPK signaling pathways, were closely associated with osteogenic differentiation. KEGG: Kyoto Encyclopedia of Genes and Genomes; TGF-β: transforming growth factor-β; MAPK: mitogen-activated protein kinase.

MYB, PRICKLE1, SEMA6A, SEMA6D, and *SOX6*) and downregulated genes (*SHC4* and *SOX17*) being involved. The term for mesenchymal cell differentiation included both upregulated genes (*BMP4, EDN1, KBTBD8, RGCC, SEMA6A, SEMA6D,* and *ZNF703*) and downregulated genes (*HEY1* and *LDLRAD4*). The most significantly enriched molecular function (MF) terms included R-SMAD binding, SMAD binding, I-SMAD binding, signaling receptor activator activity, and receptor ligand activity (**Figure 3D**). Collectively, the results suggest that the transforming growth factor (TGF)-β/BMP-SMAD signaling pathway plays a pivotal role in the induction of osteogenic differentiation by MOS in HUC-MSCs.

A total of 72 genes were mapped onto signaling pathways, as determined using the KEGG pathway enrichment analysis. The TGF-β, calcium, and mitogen-activated protein kinase (MAPK) signaling pathways were among the 19 pathways that were significantly enriched (**Figure 4**). Notably, the TGF-β signaling pathway emerged as an essential pathway, aligning with the enriched biological terms for SMAD mentioned above.

MOS promoted osteogenic differentiation via BMP-SMAD signaling

To investigate the mechanisms underlying the MOS-induced osteogenic differentiation of HUC-MSCs, we treated cells with the BMP pathway inhibitor Noggin, in combination with MOS, and used BMP4 as the positive control. Western blotting was used to analyze the changes in p-SMAD1/5/9 protein expression levels (**Figure 5A**), while RT-qPCR was used to quantify the mRNA expression of the osteogenic markers *OCN*, *OPN*, and *RUNX2* (**Figure 5B**). Western blot analysis showed increased p-SMAD1/5/9 protein expression levels in the OM+MOS group and that the addition of Noggin reversed this increase. In addition, RT-qPCR results showed a significant increase in the expression of osteogenesis-specific genes in the OM+MOS group; however, the expression of these genes was significantly reduced in the OM+MOS+Noggin group. These results confirmed the influence of MOS on the BMP-SMAD signaling pathway.

Discussion

The clinical application of MSCs depends on their ability to differentiate into multiple cell types, including osteoblasts, adipocytes, and chondrocytes, and their potential for self-renewal [3, 21]. HUC-MSCs are widely used in experimental studies to analyze *in vitro* osteogenic differentiation potential [22, 23]. Numerous studies have shown that some traditional herbal medicines can significantly improve the osteogenic differentiation ability of MSCs during osteogenic differentiation [22]. Previous studies have demonstrated that certain carbohydrate components, such as polysaccharides and oligosaccharides of *M. officinalis*, are crucial for the prevention and treatment of osteoporosis [18, 24-26]. However, no experimental study has determined whether MOS can pro-

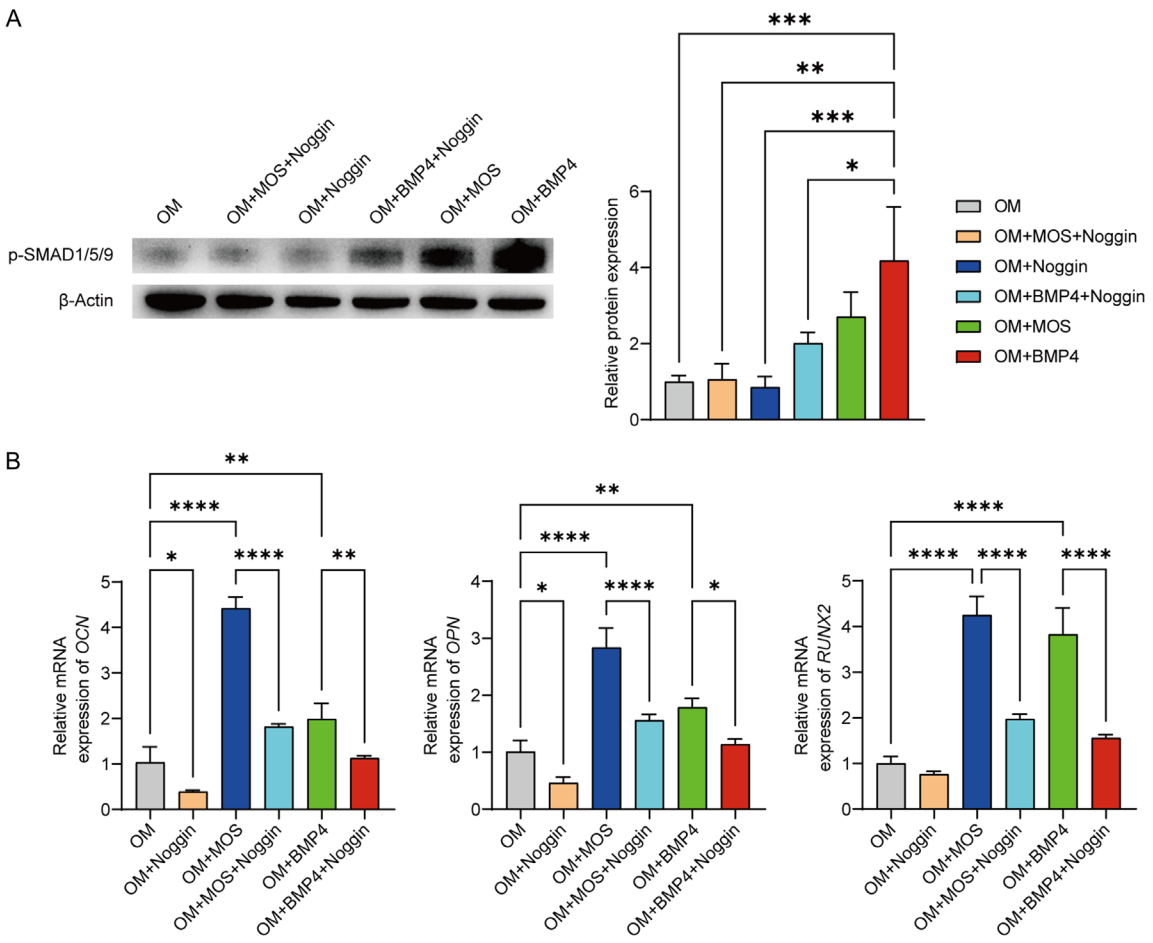

Figure 5. MOS-induced osteogenic differentiation of HUC-MSCs via the BMP-SMAD signaling pathway. A. HUC-MSCs were cultured for 24 h. Changes in p-SMAD1/5/9 protein expression levels were detected using western blotting. p-SMAD1/5/9 protein expression in HUC-MSCs was quantified using ImageJ and normalized to β-actin expression. B. RT-qPCR analysis of mRNA levels in HUC-MSCs treated for six days. Data are presented as mean ± SD; n = 3 (*P < 0.05, **P < 0.01, ***P < 0.001, ****P < 0.0001). Significant differences were analyzed using a one-way ANOVA with Tukey's post-hoc test. MOS: *Morinda officinalis* saponins; HUC-MSCs: human umbilical cord-derived mesenchymal stem cells; RT-qPCR: quantitative reverse transcription-PCR; SD: standard deviation.

mote the osteogenic differentiation of HUC-MSCs. Furthermore, little is known regarding the molecular mechanisms through which MOS promote osteogenic differentiation.

The directed differentiation of MSCs is regulated by several intracellular signaling pathways and transcription factors [27]. BMP4, a member of the TGF-β superfamily, is a growth factor that actively contributes to bone formation [28]. Multiple members of the TGF-β signaling family can regulate the differentiation of MSCs into specific cells by influencing the activity and expression of key transcription factors [29-31]. Except for BMP3, all other BMPs generally promote the osteogenic differentiation of MSCs [32-34]. In this study, *BMP4* was significantly upregulated after MOS treatment, which is consistent with our experimental results regarding the induction of osteogenic differentiation in HUC-MSCs by MOS. In addition, the expression of *CXCR4* [35], *FGF5* [36], and *ADRB2* [37], which promote the osteogenic differentiation of MSCs, significantly increased. Notably, apart from the expression of positive regulators of osteogenic differentiation, the expression of SMAD6 [38] and ID1 [39], which are known to negatively regulate the osteogenic differentiation of MSCs, was reduced after MOS treatment. Previous studies have shown that the differentiation of MSCs into osteoblasts is accompanied by the expression of Ca^{2+}-binding proteins [40], and calcium signaling is activated during MSC osteogenic differentiation [41].

The MAPK signaling pathway is a major signal transducer that regulates the osteogenic differentiation of MSCs [42]; suppression of the MAPK signaling pathway leads to a significant reduction in the expression of osteogenesis-related genes [43]. MAPK is the only active signaling molecule involved in the regulation of the three MSC differentiation lineages (osteogenic, adipogenic, and chondrogenic lineages) [44]. In the present study, the TGF-β, calcium, and MAPK signaling pathways were significantly enriched at the transcriptome level after MOS treatment.

The TGF-β superfamily comprises TGF-β, BMP, activins, and related proteins [45]. In the canonical SMAD pathway, BMP2 and BMP4 ligands can phosphorylate the downstream mediators SMAD1, SMAD5, and SMAD9 by binding to the BMP receptor complex at the cell surface and then forming a complex with SMAD4, which is translocated into the nucleus to activate osteogenic genes to stimulate osteoclast differentiation [46, 47]. Therefore, we selected BMP4 as a positive control for the promotion of osteoclast differentiation through BMP signaling. Noggin's primary structure consists of an acidic amino-terminal and a cysteine-rich carboxy-terminal region. This clip snakes around the BMP ligand and occludes the surfaces of the growth factor from binding to both the BMP types I and II receptors, thereby acting as an efficient antagonist of BMP signaling [48]. Our results showed that Noggin significantly reduced the effects of MOS on osteogenic differentiation and osteogenesis-related gene expression. These findings suggest that MOS can promote osteogenic differentiation through the BMP-SMAD signaling pathway.

Although our study elucidated the osteogenic effects of MOS on HUC-MSCs, it is essential to acknowledge that *in vitro* findings may not fully replicate the complex *in vivo* microenvironment. Future investigations incorporating animal models and clinical trials are warranted to validate the translational potential of MOS in osteoporosis treatment.

Conclusion

Our study provides a molecular basis that enhances our understanding of the mechanisms through which MOS promote the osteogenic differentiation of HUC-MSCs, thereby providing novel insights into the application of MOS in MSC-based treatments for bone diseases. Overall, MOS can partially promote the osteogenic differentiation of HUC-MSCs through the BMP-SMAD signaling pathway, which suggests that MOS are promising agents for the prevention and adjunct treatment of osteoporosis using stem cell therapy. Future studies should explore the long-term effects and safety profiles of MOS *in vivo* and address questions related to optimal dosage, potential side effects, and sustained efficacy. Additionally, investigating the synergistic effects of MOS in combination with other osteogenic agents or pharmaceuticals could enhance the understanding of their therapeutic applications in bone regeneration and osteoporosis management.

Acknowledgements

This work was supported by Jiangxi Natural Science Foundation for distinguished young scholars (20212ACB216001), Startup Foundation for Advanced Talents (QD201910), Jiangxi key research and development program (20203BBG73063), Jiangxi Double Thousand Plan (jxsq2019101064), Graduate Innovation Special Fund project of Jiangxi Education Department (YC2021-S804), Liaoning Revitalization Talents Program (XLYC2002027), Construction of Liaoning technological innovation center (1590826279052), Central government funds for guiding local scientific and Technological Development (2021JH6/10500225), Scientific Research Fund of Education Department of Liaoning Province in 2021 (LJKZ0464), and Young Scientists Nurturing Program from Department of Education of Liaoning Province (LQ2020022).

Disclosure of conflict of interest

None.

Address correspondence to: Xiushan Yin, Applied Biology Laboratory, College of Pharmaceutical and Biological Engineering, Shenyang University of Chemical Technology, No. 13 Road, Tiexi District, Shenyang 110142, Liaoning, China. E-mail: xiushanyin@me.com; Jian Li, College of Pharmaceutical Sciences, Gannan Medical University, No. 1 Medical College Road, Ganzhou 341000, Jiangxi, China. E-mail: lijian@gmu.edu.cn

References

[1] Hass R, Kasper C, Böhm S and Jacobs R. Different populations and sources of human mesenchymal stem cells (MSC): a comparison of adult and neonatal tissue-derived MSC. Cell Commun Signal 2011; 9: 12.

[2] Almalki SG and Agrawal DK. Key transcription factors in the differentiation of mesenchymal stem cells. Differentiation 2016; 92: 41-51.

[3] Pittenger MF, Mackay AM, Beck SC, Jaiswal RK, Douglas R, Mosca JD, Moorman MA, Simonetti DW, Craig S and Marshak DR. Multilineage potential of adult human mesenchymal stem cells. Science 1999; 284: 143-147.

[4] Zhang LB and He M. Effect of mesenchymal stromal (stem) cell (MSC) transplantation in asthmatic animal models: a systematic review and meta-analysis. Pulm Pharmacol Ther 2019; 54: 39-52.

[5] Harrell CR, Markovic BS, Fellabaum C, Arsenijevic A and Volarevic V. Mesenchymal stem cell-based therapy of osteoarthritis: current knowledge and future perspectives. Biomed Pharmacother 2019; 109: 2318-2326.

[6] Han B, Zhou L, Guan Q, da Roza G, Wang H and Du C. *In vitro* expansion and characterization of mesenchymal stromal cells from peritoneal dialysis effluent in a human protein medium. Stem Cells Int 2018; 2018: 5868745.

[7] Prockop DJ. Marrow stromal cells as stem cells for nonhematopoietic tissues. Science 1997; 276: 71-74.

[8] Xu J, Liu G, Wang X, Hu Y, Luo H, Ye L, Feng Z, Li C, Kuang M, Zhang L, Zhou Y and Qi X. hUC-MSCs: evaluation of acute and long-term routine toxicity testing in mice and rats. Cytotechnology 2022; 74: 17-29.

[9] Li T, Xia M, Gao Y, Chen Y and Xu Y. Human umbilical cord mesenchymal stem cells: an overview of their potential in cell-based therapy. Expert Opin Biol Ther 2015; 15: 1293-1306.

[10] Shu L, Niu C, Li R, Huang T, Wang Y, Huang M, Ji N, Zheng Y, Chen X, Shi L, Wu M, Deng K, Wei J, Wang X, Cao Y, Yan J and Feng G. Treatment of severe COVID-19 with human umbilical cord mesenchymal stem cells. Stem Cell Res Ther 2020; 11: 361.

[11] Zhu J, Peng Q, Xu Y, Xu H, Wan Y, Li Z, Qiu Y, Xia W, Guo Z, Li H, Jin H and Hu B. Morinda officinalis oligosaccharides ameliorate depressive-like behaviors in poststroke rats through upregulating GLUT3 to improve synaptic activity. FASEB J 2020; 34: 13376-13395.

[12] Yang YJ, Shu HY and Min ZD. Anthraquinones isolated from Morinda officinalis and Damnacanthus indicus. Yao Xue Xue Bao 1992; 27: 358-364.

[13] Wu YB, Zheng CJ, Qin LP, Sun LN, Han T, Jiao L, Zhang QY and Wu JZ. Antiosteoporotic activity of anthraquinones from Morinda officinalis on osteoblasts and osteoclasts. Molecules 2009; 14: 573-583.

[14] Li Z, Xu H, Xu Y, Lu G, Peng Q, Chen J, Bi R, Li J, Chen S, Li H, Jin H and Hu B. Morinda officinalis oligosaccharides alleviate depressive-like behaviors in post-stroke rats via suppressing NLRP3 inflammasome to inhibit hippocampal inflammation. CNS Neurosci Ther 2021; 27: 1570-1586.

[15] Yan C, Huang D, Shen X, Qin N, Jiang K, Zhang D and Zhang Q. Identification and characterization of a polysaccharide from the roots of Morinda officinalis, as an inducer of bone formation by up-regulation of target gene expression. Int J Biol Macromol 2019; 133: 446-456.

[16] Seo BI, Ku SK, Cha EM, Park JH, Kim JD, Choi HY and Lee HS. Effect of Mornidae Radix extracts on experimental osteoporosis in sciatic neurectomized mice. Phytother Res 2005; 19: 231-238.

[17] Zhang JH, Xin HL, Xu YM, Shen Y, He YQ, Hsien-Yeh, Lin B, Song HT, Juan-Liu, Yang HY, Qin LP, Zhang QY and Du J. Morinda officinalis How. - A comprehensive review of traditional uses, phytochemistry and pharmacology. J Ethnopharmacol 2018; 213: 230-255.

[18] He YQ, Zhang Q, Shen Y, Han T, Zhang QL, Zhang JH, Lin B, Song HT, Hsu HY, Qin LP, Xin HL and Zhang QY. Rubiadin-1-methyl ether from Morinda officinalis How. Inhibits osteoclastogenesis through blocking RANKL-induced NF-κB pathway. Biochem Biophys Res Commun 2018; 506: 927-931.

[19] Zhang L, Zhao X and Wang W. lncRNA and mRNA sequencing of the left testis in experimental varicocele rats treated with Morinda officinalis polysaccharide. Exp Ther Med 2021; 22: 1136.

[20] Livak KJ and Schmittgen TD. Analysis of relative gene expression data using real-time quantitative PCR and the 2(-delta delta C(T)) method. Methods 2001; 25: 402-408.

[21] Dominici M, Le Blanc K, Mueller I, Slaper-Cortenbach I, Marini F, Krause D, Deans R, Keating A, Prockop Dj and Horwitz E. Minimal criteria for defining multipotent mesenchymal stromal cells. The International Society for Cellular Therapy position statement. Cytotherapy 2006; 8: 315-317.

[22] He S, Yang S, Zhang Y, Li X, Gao D, Zhong Y, Cao L, Ma H, Liu Y, Li G, Peng S and Shuai C. LncRNA ODIR1 inhibits osteogenic differentiation of hUC-MSCs through the FBXO25/H2B-K120ub/H3K4me3/OSX axis. Cell Death Dis 2019; 10: 947.

[23] Hendrijantini N and Hartono P. Phenotype characteristics and osteogenic differentiation potential of human mesenchymal stem cells derived from Amnion Membrane (HAMSCs) and Umbilical Cord (HUC-MSCs). Acta Inform Med 2019; 27: 72-77.
[24] Zhang D, Zhang S, Jiang K, Li T and Yan C. Bioassay-guided isolation and evaluation of anti-osteoporotic polysaccharides from Morinda officinalis. J Ethnopharmacol 2020; 261: 113113.
[25] Xia T, Dong X, Lin L, Jiang Y, Ma X, Xin H, Zhang Q and Qin L. Metabolomics profiling provides valuable insights into the underlying mechanisms of Morinda officinalis on protecting glucocorticoid-induced osteoporosis. J Pharm Biomed Anal 2019; 166: 336-346.
[26] Jiang K, Huang D, Zhang D, Wang X, Cao H, Zhang Q and Yan C. Investigation of inulins from the roots of Morinda officinalis for potential therapeutic application as anti-osteoporosis agent. Int J Biol Macromol 2018; 120: 170-179.
[27] Sun Q, Liu S, Feng J, Kang Y, Zhou Y and Guo S. Current status of MicroRNAs that target the Wnt signaling pathway in regulation of osteogenesis and bone metabolism: a review. Med Sci Monit 2021; 27: e929510.
[28] Seeherman HJ, Berasi SP, Brown CT, Martinez RX, Juo ZS, Jelinsky S, Cain MJ, Grode J, Tumelty KE, Bohner M, Grinberg O, Orr N, Shoseyov O, Eyckmans J, Chen C, Morales PR, Wilson CG, Vanderploeg EJ and Wozney JM. A BMP/activin A chimera is superior to native BMPs and induces bone repair in nonhuman primates when delivered in a composite matrix. Sci Transl Med 2019; 11: eaar4953.
[29] Minina E, Wenzel HM, Kreschel C, Karp S, Gaffield W, McMahon AP and Vortkamp A. BMP and Ihh/PTHrP signaling interact to coordinate chondrocyte proliferation and differentiation. Development 2001; 128: 4523-4534.
[30] Oshimori N and Fuchs E. The harmonies played by TGF-β in stem cell biology. Cell Stem Cell 2012; 11: 751-764.
[31] Grafe I, Alexander S, Peterson JR, Snider TN, Levi B, Lee B and Mishina Y. TGF-β family signaling in mesenchymal differentiation. Cold Spring Harb Perspect Biol 2018; 10: a022202.
[32] Kokabu S, Gamer L, Cox K, Lowery J, Tsuji K, Raz R, Economides A, Katagiri T and Rosen V. BMP3 suppresses osteoblast differentiation of bone marrow stromal cells via interaction with Acvr2b. Mol Endocrinol 2012; 26: 87-94.
[33] Chen D, Ji X, Harris MA, Feng JQ, Karsenty G, Celeste AJ, Rosen V, Mundy GR and Harris SE. Differential roles for bone morphogenetic protein (BMP) receptor type IB and IA in differentiation and specification of mesenchymal precursor cells to osteoblast and adipocyte lineages. J Cell Biol 1998; 142: 295-305.
[34] Liu DD, Zhang JC, Zhang Q, Wang SX and Yang MS. TGF-β/BMP signaling pathway is involved in cerium-promoted osteogenic differentiation of mesenchymal stem cells. J Cell Biochem 2013; 114: 1105-1114.
[35] Gong ZM, Tang ZY and Sun XL. LncRNA PRNCR1 regulates CXCR4 expression to affect osteogenic differentiation and contribute to osteolysis after hip replacement. Gene 2018; 673: 251-261.
[36] Park GC, Song JS, Park HY, Shin SC, Jang JY, Lee JC, Wang SG, Lee BJ and Jung JS. Role of fibroblast growth factor-5 on the proliferation of human tonsil-derived mesenchymal stem cells. Stem Cells Dev 2016; 25: 1149-1160.
[37] Alves Barreto AE, Balera Brito VG, Patrocinio MS, Ballassoni BB, Tfaile Frasnelli SC and Penha Oliveira SH. β1-adrenergic receptor but not β2 mediates osteogenic differentiation of bone marrow mesenchymal stem cells in normotensive and hypertensive rats. Eur J Pharmacol 2021; 911: 174515.
[38] Wang C, Zheng GF and Xu XF. MicroRNA-186 improves fracture healing through activating the bone morphogenetic protein signalling pathway by inhibiting SMAD6 in a mouse model of femoral fracture: an animal study. Bone Joint Res 2019; 8: 550-562.
[39] Peng Y, Kang Q, Luo Q, Jiang W, Si W, Liu BA, Luu HH, Park JK, Li X, Luo J, Montag AG, Haydon RC and He TC. Inhibitor of DNA binding/differentiation helix-loop-helix proteins mediate bone morphogenetic protein-induced osteoblast differentiation of mesenchymal stem cells. J Biol Chem 2004; 279: 32941-32949.
[40] Carlier A, Chai YC, Moesen M, Theys T, Schrooten J, Van Oosterwyck H and Geris L. Designing optimal calcium phosphate scaffold-cell combinations using an integrative model-based approach. Acta Biomater 2011; 7: 3573-3585.
[41] Viti F, Landini M, Mezzelani A, Petecchia L, Milanesi L and Scaglione S. Osteogenic differentiation of MSC through calcium signaling activation: transcriptomics and functional analysis. PLoS One 2016; 11: e0148173.
[42] Ge C, Xiao G, Jiang D and Franceschi RT. Critical role of the extracellular signal-regulated kinase-MAPK pathway in osteoblast differentiation and skeletal development. J Cell Biol 2007; 176: 709-718.
[43] Liu Q, Zhuang Y, Ouyang N and Yu H. Cytochalasin D promotes osteogenic differentiation of MC3T3-E1 cells via p38-MAPK signaling pathway. Curr Mol Med 2019; 20: 79-88.
[44] Mei Y, Bian C, Li J, Du Z, Zhou H, Yang Z and Zhao RC. miR-21 modulates the ERK-MAPK signaling pathway by regulating SPRY2 expres-

sion during human mesenchymal stem cell differentiation. J Cell Biochem 2013; 114: 1374-1384.
[45] Derynck R and Zhang YE. Smad-dependent and Smad-independent pathways in TGF-β family signalling. Nature 2003; 425: 577-584.
[46] Chen G, Deng C and Li YP. TGF-β and BMP signaling in osteoblast differentiation and bone formation. Int J Biol Sci 2012; 8: 272-288.
[47] Liu DD, Zhang CY, Liu Y, Li J, Wang YX and Zheng SG. RUNX2 regulates osteoblast differentiation via the BMP4 signaling pathway. J Dent Res 2022; 101: 1227-1237.
[48] Krause C, Guzman A and Knaus P. Noggin. Int J Biochem Cell Biol 2011; 43: 478-481.

Table S1. The result of GO enrichment including BP and MP from the DEGs

Function	ID	Description	BgRatio	*p*value	p.adjust	qvalue	geneID	Count
BP	GO:0003177	pulmonary valve development	21/18866	4.772E-07	0.0013285	0.0011267	BMP4/HEY1/SMAD6/STRA6/TNFRSF1B	5
	GO:0036293	response to decreased oxygen levels	371/18866	1.168E-06	0.0016257	0.0013788	ANKRD1/CITED2/CPEB1/CXCR4/DDAH1/DDIT4/EDN1/EGLN3/HILPDA/MYB/NDNF/OXTR/PMAIP1/RGCC	14
	GO:0070482	response to oxygen levels	396/18866	2.507E-06	0.0023268	0.0019733	ANKRD1/CITED2/CPEB1/CXCR4/DDAH1/DDIT4/EDN1/EGLN3/HILPDA/MYB/NDNF/OXTR/PMAIP1/RGCC	14
	GO:0001666	response to hypoxia	359/18866	4.492E-06	0.0024075	0.0020418	ANKRD1/CITED2/CPEB1/CXCR4/DDAH1/DDIT4/EDN1/EGLN3/HILPDA/MYB/NDNF/PMAIP1/RGCC	13
	GO:0071456	cellular response to hypoxia	208/18866	5.144E-06	0.0024075	0.0020418	ANKRD1/CITED2/CPEB1/DDAH1/EDN1/EGLN3/HILPDA/NDNF/PMAIP1/RGCC	10
	GO:0003007	heart morphogenesis	258/18866	5.439E-06	0.0024075	0.0020418	ADAMTS1/ADGRG6/ANKRD1/BMP4/CITED2/HEY1/PKP2/S1PR1/SMAD6/SOX17/SYNPO2L	11
	GO:0048863	stem cell differentiation	264/18866	6.767E-06	0.0024075	0.0020418	BMP4/EDN1/KBTBD8/KIT/MYB/PRICKLE1/SEMA6A/SEMA6D/SHC4/SOX17/SOX6	11
	GO:0003184	pulmonary valve morphogenesis	17/18866	7.574E-06	0.0024075	0.0020418	BMP4/HEY1/SMAD6/STRA6	4
	GO:0036294	cellular response to decreased oxygen levels	218/18866	7.783E-06	0.0024075	0.0020418	ANKRD1/CITED2/CPEB1/DDAH1/EDN1/EGLN3/HILPDA/NDNF/PMAIP1/RGCC	10
	GO:1905314	semi-lunar valve development	37/18866	9.252E-06	0.0025759	0.0021846	BMP4/HEY1/SMAD6/STRA6/TNFRSF1B	5
	GO:1905207	regulation of cardiocyte differentiation	66/18866	1.201E-05	0.0030406	0.0025787	BMP4/EDN1/PRICKLE1/RGS4/SOX17/SOX6	6
	GO:0071453	cellular response to oxygen levels	235/18866	1.498E-05	0.003399	0.0028827	ANKRD1/CITED2/CPEB1/DDAH1/EDN1/EGLN3/HILPDA/NDNF/PMAIP1/RGCC	10
	GO:0071902	positive regulation of protein serine/threonine kinase activity	345/18866	1.587E-05	0.003399	0.0028827	ADRB2/BMP4/CEMIP/CXCR4/DUSP5/EDN1/KIT/LPAR3/NEK10/NGF/NTF3/RGCC	12
	GO:0001558	regulation of cell growth	420/18866	2.387E-05	0.0046153	0.0039141	BDKRB1/CDKN2C/CXCR4/EDN1/HBEGF/LPAR3/NGF/NPPB/RGS4/SEMA6A/SEMA6D/SOCS2/SOX17	13
	GO:0050769	positive regulation of neurogenesis	485/18866	2.487E-05	0.0046153	0.0039141	ANKRD1/BMP4/CXCR4/KIT/LPAR3/MYB/NDNF/NGF/ROR1/SEMA6A/SOCS2/TNFRSF1B/TOX/ZNF804A	14
	GO:0071560	cellular response to transforming growth factor beta stimulus	252/18866	2.73E-05	0.0047505	0.0040288	ANKRD1/CITED2/EDN1/ID1/LDLRAD4/SMAD6/SMAD9/SMURF2/SOX6/ZNF703	10
	GO:0045926	negative regulation of growth	254/18866	2.92E-05	0.0047827	0.0040561	ADRB2/BDKRB1/BMP4/CDKN2C/NPPB/RGS4/SEMA6A/SEMA6D/SOCS2/SOX17	10
	GO:0071559	response to transforming growth factor beta	258/18866	3.335E-05	0.0051413	0.0043602	ANKRD1/CITED2/EDN1/ID1/LDLRAD4/SMAD6/SMAD9/SMURF2/SOX6/ZNF703	10
	GO:0045446	endothelial cell differentiation	117/18866	3.509E-05	0.0051413	0.0043602	ATOH8/BMP4/CXCR4/HEY1/ID1/S1PR1/SOX17	7
	GO:0050954	sensory perception of mechanical stimulus	173/18866	6.119E-05	0.0084483	0.0071648	ATP8B1/CEMIP/CXCR4/KIT/MBP/ROR1/TFAP2A/USP53	8
	GO:0003205	cardiac chamber development	174/18866	6.373E-05	0.0084483	0.0071648	ADAMTS1/ADGRG6/BMP4/CITED2/HEY1/PKP2/SMAD6/STRA6	8
	GO:0003206	cardiac chamber morphogenesis	131/18866	7.217E-05	0.0086822	0.0073632	ADAMTS1/ADGRG6/BMP4/CITED2/HEY1/PKP2/SMAD6	7
	GO:0043405	regulation of MAP kinase activity	342/18866	7.336E-05	0.0086822	0.0073632	BMP4/CXCR4/DUSP5/DUSP8/EDN1/KIT/LPAR3/NEK10/NGF/NTF3/RGS4	11
	GO:0048762	mesenchymal cell differentiation	229/18866	7.485E-05	0.0086822	0.0073632	BMP4/EDN1/HEY1/KBTBD8/LDLRAD4/RGCC/SEMA6A/SEMA6D/ZNF703	9

	GO:0003158	endothelium development	135/18866	8.725E-05	0.009509	0.0080644	ATOH8/BMP4/CXCR4/HEY1/ID1/S1PR1/SOX17	7
	GO:0060485	mesenchyme development	290/18866	8.88E-05	0.009509	0.0080644	BMP4/CITED2/EDN1/HEY1/KBTBD8/ LDLRAD4/RGCC/SEMA6A/SEMA6D/ZNF703	10
	GO:0003073	regulation of systemic arterial blood pressure	95/18866	9.562E-05	0.0098597	0.0083618	ADRB2/DDAH1/EDN1/NPPB/OXTR/SLC2A5	6
	GO:0003170	heart valve development	61/18866	0.0001088	0.0108168	0.0091735	BMP4/HEY1/SMAD6/STRA6/TNFRSF1B	5
	GO:0016049	cell growth	490/18866	0.0001147	0.0110069	0.0093347	BDKRB1/CDKN2C/CXCR4/EDN1/HBEGF/LPAR3/ NGF/NPPB/RGS4/SEMA6A/SEMA6D/SOCS2/SOX17	13
	GO:0051482	positive regulation of cytosolic calcium ion concentration involved in phospholipase C-activating G protein-coupled signaling pathway	34/18866	0.0001333	0.0119667	0.0101487	EDN1/F2RL2/LPAR3/S1PR1	4
MF	GO:0070412	R-SMAD binding	23/18352	3.026E-05	0.0070382	0.0063918	ANKRD1/LDLRAD4/RGCC/SMAD6	4
	GO:0046332	SMAD binding	79/18352	3.943E-05	0.0070382	0.0063918	ANKRD1/LDLRAD4/RGCC/SMAD6/ SMAD9/SMURF2	6
	GO:0005539	glycosaminoglycan binding	232/18352	0.0005459	0.064967	0.0589999	ADAMTS1/ADAMTS15/BMP4/CEMIP/ CXCL6/HBEGF/NDNF/TNFAIP6	8
	GO:0048018	receptor ligand activity	487/18352	0.0018027	0.1128224	0.10246	BMP4/CCL20/CXCL6/EDN1/FGF5/HBEGF/ NGF/NPPB/NTF3/SEMA6A/SEMA6D	11
	GO:0030546	signaling receptor activator activity	492/18352	0.0019526	0.1128224	0.10246	BMP4/CCL20/CXCL6/EDN1/FGF5/HBEGF/ NGF/NPPB/NTF3/SEMA6A/SEMA6D	11
	GO:0008201	heparin binding	169/18352	0.0023412	0.1128224	0.10246	ADAMTS1/ADAMTS15/BMP4/CXCL6/ HBEGF/NDNF	6
	GO:0008330	protein tyrosine/threonine phosphatase activity	10/18352	0.0027127	0.1128224	0.10246	DUSP5/DUSP8	2
	GO:0032052	bile acid binding	10/18352	0.0027127	0.1128224	0.10246	AKR1C1/AKR1C2	2
	GO:0016813	hydrolase activity, acting on carbon-nitrogen (but not peptide) bonds, in linear amidines	11/18352	0.0032983	0.1128224	0.10246	DDAH1/PADI1	2
	GO:0004032	alditol:NADP+ 1-oxidoreductase activity	12/18352	0.0039374	0.1128224	0.10246	AKR1C1/AKR1C2	2
	GO:0005165	neurotrophin receptor binding	12/18352	0.0039374	0.1128224	0.10246	NGF/NTF3	2
	GO:0017017	MAP kinase tyrosine/serine/threonine phosphatase activity	13/18352	0.004629	0.1128224	0.10246	DUSP5/DUSP8	2
	GO:0030548	acetylcholine receptor regulator activity	13/18352	0.004629	0.1128224	0.10246	LYPD6/LYPD6B	2
	GO:0099602	neurotransmitter receptor regulator activity	13/18352	0.004629	0.1128224	0.10246	LYPD6/LYPD6B	2
	GO:1901681	sulfur compound binding	262/18352	0.0050388	0.1128224	0.10246	ADAMTS1/ADAMTS15/BMP4/CXCL6/ HBEGF/NDNF/PTGES	7
	GO:0033549	MAP kinase phosphatase activity	14/18352	0.0053725	0.1128224	0.10246	DUSP5/DUSP8	2
	GO:0070411	I-SMAD binding	14/18352	0.0053725	0.1128224	0.10246	SMAD6/SMAD9	2
	GO:0005126	cytokine receptor binding	271/18352	0.0060354	0.1197027	0.1087084	CCL20/CXCL6/NGF/NTF3/SMAD6/ SMURF2/SOCS2	7
	GO:0045125	bioactive lipid receptor activity	16/18352	0.0070113	0.1257985	0.1142443	LPAR3/S1PR1	2
	GO:0031406	carboxylic acid binding	212/18352	0.0070475	0.1257985	0.1142443	AKR1C1/AKR1C2/CEMIP/DDAH1/ EGLN3/TNFAIP6	6
	GO:0043177	organic acid binding	224/18352	0.0091159	0.1549706	0.140737	AKR1C1/AKR1C2/CEMIP/DDAH1/ EGLN3/TNFAIP6	6
	GO:0008083	growth factor activity	162/18352	0.0095943	0.1556896	0.1413899	BMP4/FGF5/HBEGF/NGF/NTF3	5
	GO:0005123	death receptor binding	20/18352	0.0108729	0.1687657	0.1532651	NGF/NTF3	2

GO:0008106	alcohol dehydrogenase (NADP+) activity	21/18352	0.0119552	0.1731651	0.1572604	AKR1C1/AKR1C2	2
GO:0098631	cell adhesion mediator activity	60/18352	0.0121264	0.1731651	0.1572604	MADCAM1/NEXN/PKP2	3
GO:0005540	hyaluronic acid binding	22/18352	0.0130827	0.1796362	0.1631371	CEMIP/TNFAIP6	2
GO:0030215	semaphorin receptor binding	23/18352	0.0142547	0.1884788	0.1711675	SEMA6A/SEMA6D	2
GO:0005160	transforming growth factor beta receptor binding	24/18352	0.0154703	0.1904446	0.1729528	SMAD6/SMURF2	2
GO:0070696	transmembrane receptor protein serine/threonine kinase binding	24/18352	0.0154703	0.1904446	0.1729528	BMP4/SMAD6	2
GO:0001965	G-protein alpha-subunit binding	26/18352	0.0180294	0.2011404	0.1826662	LPAR3/RGS4	2

Table S2. The result of KEGG enrichment from the DEGs

ID	Description	BgRatio	*p*value	p.adjust	qvalue	geneID	Count
hsa04350	TGF-beta signaling pathway	94/8115	0.0014218	0.1491827	0.138030287	BMP4/ID1/SMAD6/SMAD9/SMURF2	5
hsa04015	Rap1 signaling pathway	210/8115	0.002491	0.1491827	0.138030287	EFNA4/FGF5/ID1/KIT/LPAR3/NGF/PLCB4	7
hsa04924	Renin secretion	69/8115	0.0031891	0.1491827	0.138030287	ADRB2/EDN1/GUCY1A2/PLCB4	4
hsa04080	Neuroactive ligand-receptor interaction	353/8115	0.0038008	0.1491827	0.138030287	ADRB2/BDKRB1/EDN1/F2RL2/LPAR3/LYPD6/LYPD6B/OXTR/S1PR1	9
hsa04020	Calcium signaling pathway	240/8115	0.0052076	0.1635191	0.151294915	ADRB2/BDKRB1/CXCR4/FGF5/NGF/OXTR/PLCB4	7
hsa04072	Phospholipase D signaling pathway	148/8115	0.0099075	0.2460824	0.227686046	CYTH3/KIT/LPAR3/PLCB4/SHC4	5
hsa04061	Viral protein interaction with cytokine and cytokine receptor	100/8115	0.0117809	0.2460824	0.227686046	CCL20/CXCL6/CXCR4/TNFRSF1B	4
hsa04151	PI3K-Akt signaling pathway	354/8115	0.0126935	0.2460824	0.227686046	DDIT4/EFNA4/FGF5/KIT/LPAR3/MYB/NGF/NTF3	8
hsa04010	MAPK signaling pathway	294/8115	0.0150276	0.2460824	0.227686046	DUSP5/DUSP8/EFNA4/FGF5/KIT/NGF/NTF3	7
hsa04014	Ras signaling pathway	232/8115	0.0166325	0.2460824	0.227686046	EFNA4/FGF5/KIT/NGF/NTF3/SHC4	6
hsa04668	TNF signaling pathway	112/8115	0.0172414	0.2460824	0.227686046	CCL20/CXCL6/EDN1/TNFRSF1B	4
hsa04360	Axon guidance	182/8115	0.022419	0.2933146	0.271387335	CXCR4/EFNA4/SEMA6A/SEMA6D/TRPC4	5
hsa04062	Chemokine signaling pathway	192/8115	0.0274618	0.3316535	0.306860108	CCL20/CXCL6/CXCR4/PLCB4/SHC4	5
hsa04270	Vascular smooth muscle contraction	134/8115	0.0308559	0.3460269	0.320158954	EDN1/GUCY1A2/NPPB/PLCB4	4
hsa04915	Estrogen signaling pathway	138/8115	0.0338572	0.3543722	0.327880368	HBEGF/KRT34/PLCB4/SHC4	4
hsa04610	Complement and coagulation cascades	85/8115	0.039441	0.3804648	0.352022455	BDKRB1/F2RL2/F3	3
hsa05224	Breast cancer	147/8115	0.0412163	0.3804648	0.352022455	FGF5/HEY1/KIT/SHC4	4
hsa04060	Cytokine-cytokine receptor interaction	295/8115	0.0462678	0.3804648	0.352022455	BMP4/CCL20/CXCL6/CXCR4/NGF/TNFRSF1B	6
hsa04970	Salivary secretion	93/8115	0.0493109	0.3804648	0.352022455	ADRB2/GUCY1A2/PLCB4	3